Developing Long-Wave Infrared HgCdTe Detector Arrays for Future Space Missions

Mario S. Cabrera

Supervised by William J. Forrest, Judith L. Pipher, and Craig McMurtry

Monday, December 3, 2018

Outline

- Motivation
- HgCdTe
- Characterization
- Previous Work
- Current Results
- Future Work/Summary

MOTIVATION

Astronomical Motivation

- Atmosphere of Exoplanets
  - CO_2 (strong feature at 15 μm) can be used to identify terrestrial planets
  - Possibility for life shown by H_2O
    - 9.6 μm O_3 indicates abundant life
- Ocean detection in outer solar system (ice-plate tectonics on Europa, H_2O geysers on Enceladus)
- Accessibility to N-band for ground based observations

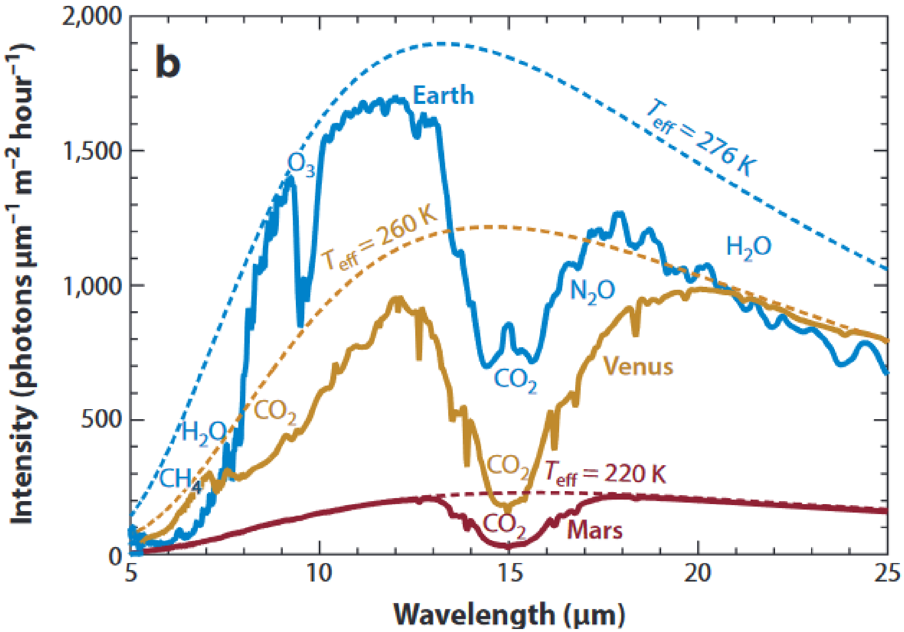

Figure Source: Kaltenegger 2017

HgCdTe

- $Hg_{1-x}Cd_xTe$
  - x composition parameter (molar concentration of Cd)
- Tunable energy band-gap
  - $E_g(x,T) = -0.302 + 1.93x - 0.81x^2 + 0.832x^3 + 5.35 \times 10^{-4}T(1-2x)$ (Hansen and Schmit 1983)
  - $E_g = \frac{hc}{\lambda_c}$
- UR infrared detector team along with JPL and Teledyne Imaging Systems have developed HgCdTe 10 μm cut-off arrays
  - NEOCam (Mainzer 2015)
    - Operabilities > 90% at a temperature of 40 K
      - Dark Current < 200 e^-/s and well depth > 44 ke^-
      - Median dark current at 40 K < 1 e^-/s (Dorn et al. 2018)
- 15 μm goal (LW15 arrays)
  - 13 μm (LW13 arrays) intermediate step

CHARACTERIZATION

Characterization

- Capacitance
- Non-Linearity
- Read-Noise
- Operability
  - Dark current
  - Well depth
  - Focus of this talk

Dark Current vs. Well Depth

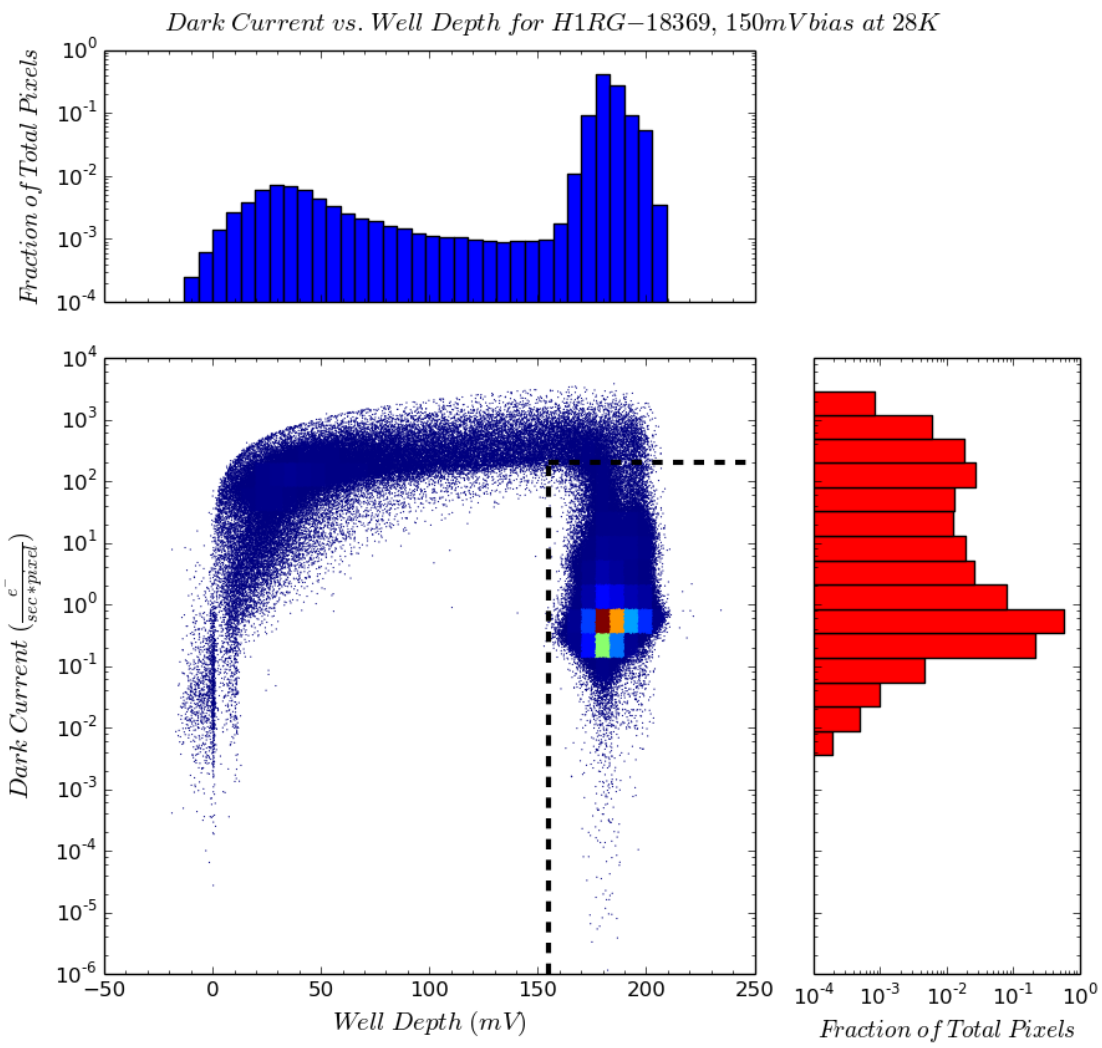

- High dark current pixels will debias considerably before first read, showing smaller dark currents
  - Inoperable pixels can then be determined through the low well depth

PREVIOUS WORK (LW13 PHASE)

- Received four LW13 cut-off detectors
  - H1RG-18367 and 18508 were grown and processed in the same manner as the 10 μm arrays for NEOCam
  - H1RG-18369 and H1RG-18509 were designed to mitigate quantum tunneling dark currents

Detector H1RG-	Wafer 2-	Lot-Split	Cut-off Wavelength (μm)	QE (6-10 μm)
18367	3757	Standard	12.8	74%
18508	3755	Standard	12.7	73%
18369	3763	Design 1	12.4	72%
18509	3759	Design 2	12.6	73%

Cabrera et al. 2019

Dark Current vs. Well Depth

- The majority of pixels for H1RG-18369, 18508, and 18509 had dark currents below $1\frac{e^-}{s}$ (Comparable to the performance of the NEOCam arrays)

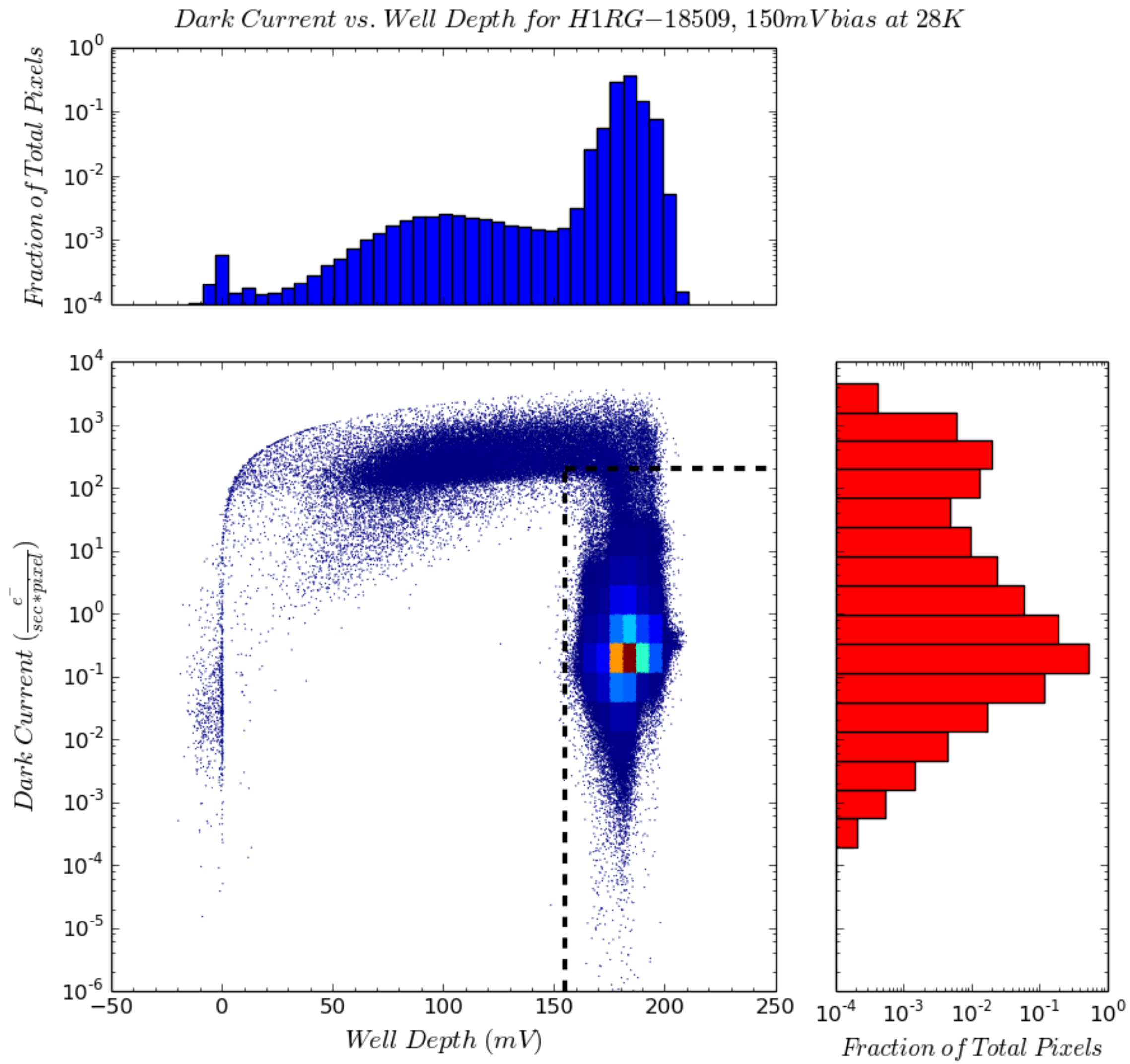

Operability Map

- Trap-band quantum tunneling dark currents occur when the arrays have traps due to defects and dislocations in the depletion region
- A mismatch between the CdZnTe substrate crystal axes and the HgCdTe layers creates cross-hatching pattern

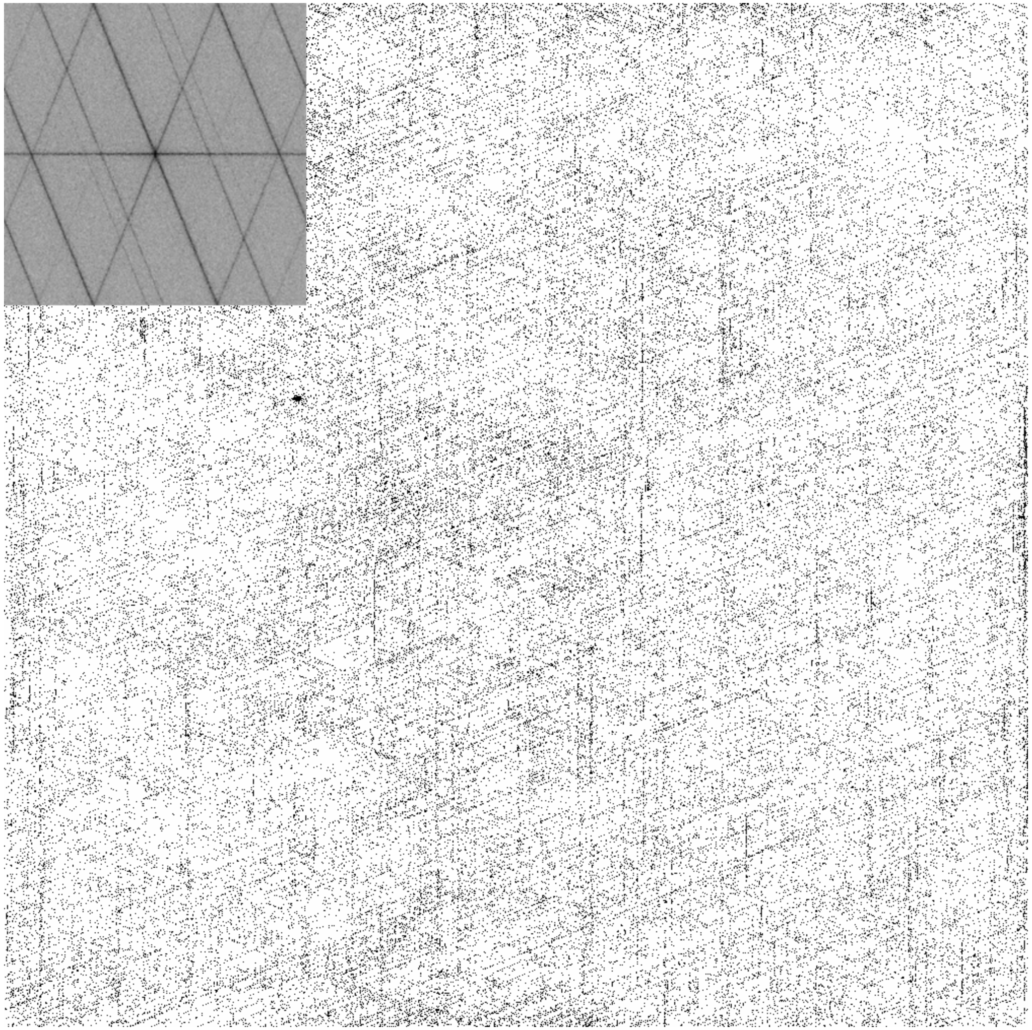

Cabrera et al. 2019

H1RG-18508 SUTR Curvature

- $I_{dark}(150\ mV) = 0.44\ e^{-}/s$
  - $Well = 45ke^{-}/174\ mV$
- $I_{dark}(250\ mV) = 35.7\ e^{-}/s$
  - $Well\ = 64ke^{-}, 271\ mV$
- $I_{dark}(350\ mV) = 787.6\ e^{-}/s$
  - $Well = 74ke^{-}, 331\ mV$

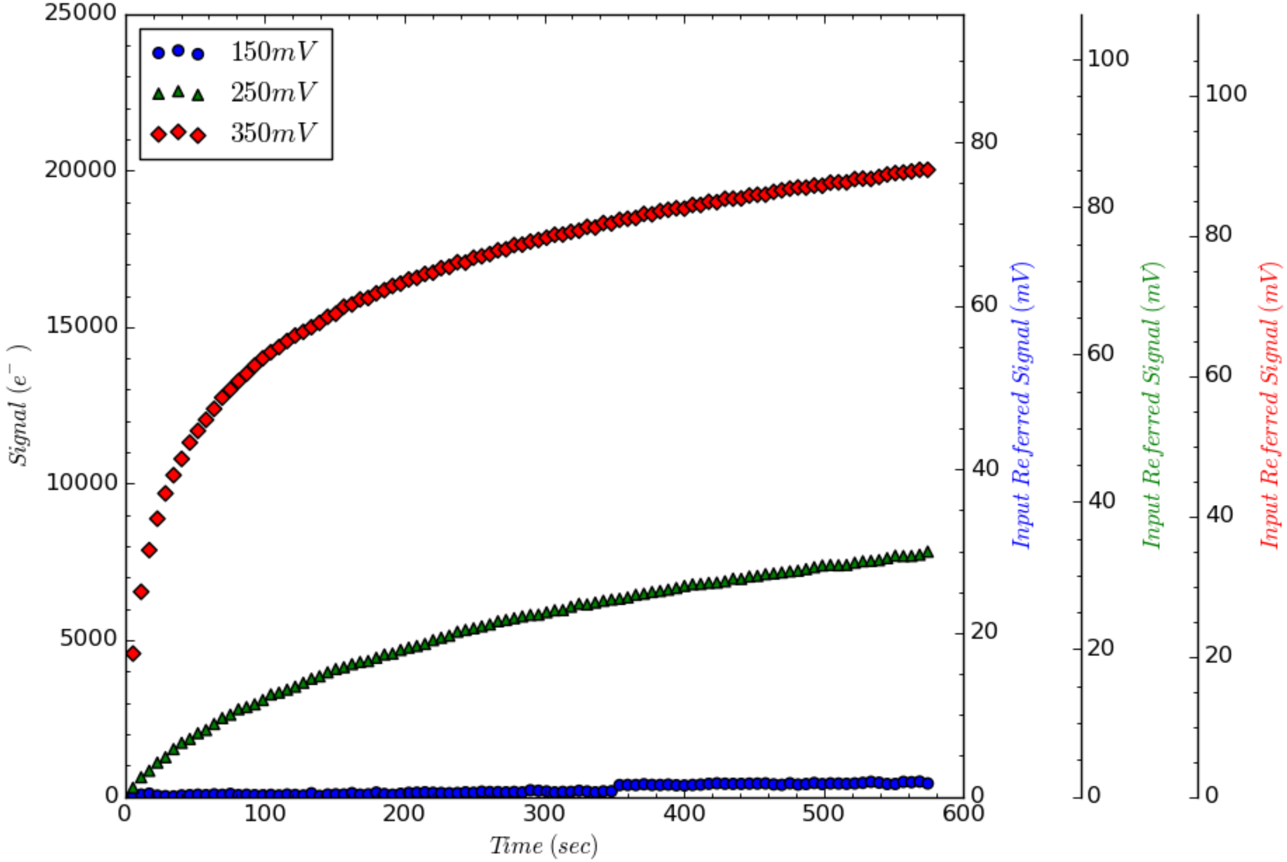

Thermally Generated Currents

- Diffusion Current (Reine et al. 1981)
  - Direct band-gap thermally generated electron-hole pairs
- Generation Recombination (G-R) current (Sah et al. 1957)
  - Trap assisted thermally generated currents

Tunneling Currents

- Band-to-band tunneling current
  - Electrons tunnel from the valence to the conduction band
- Trap-to-band tunneling current
  - Electrons tunnel from the valence to the conduction band indirectly by using intermediate traps
- Both are heavily bias dependent
  - Sze 1981
  - Kinch 1981
  - Kinch 2014

I-T with 250 mV of applied bias

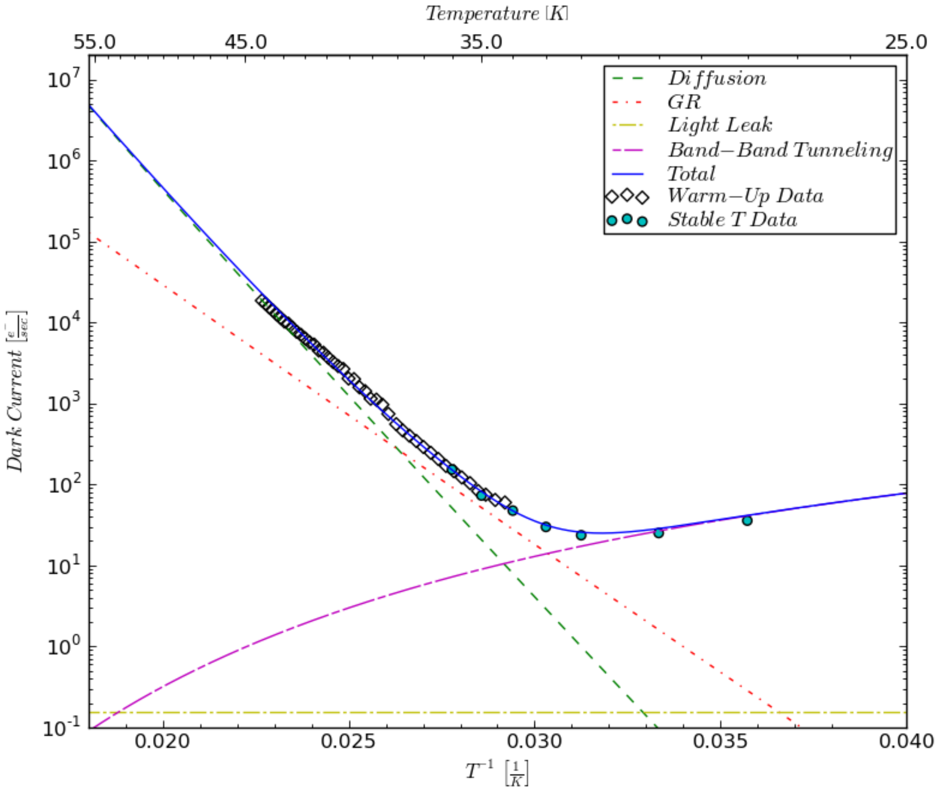

I-V at a temperature of 28 K

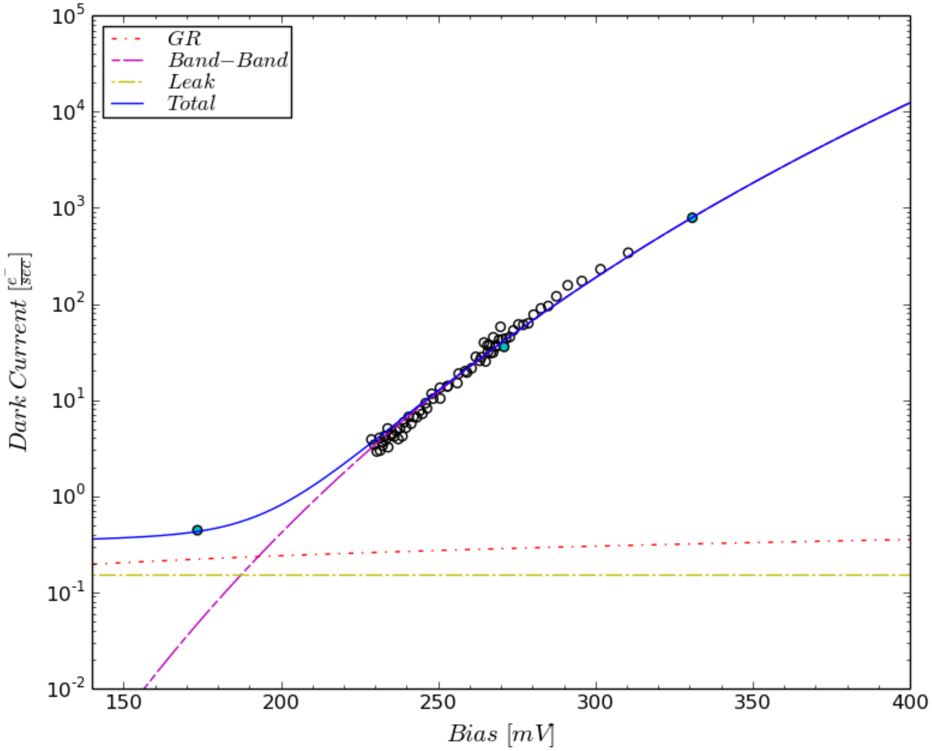

- Dark current model for pixel in previous slide

H1RG-18509 SUTR Curvature

- $I_{dark}(150\ mV) = 0.18\ e^-/s$
  - $Well = 44ke^-/180\ mV$
- $I_{dark}(250\ mV) = 0.22\ e^-/s$
  - $Well = 64ke^-, 280\ mV$
- $I_{dark}(350\ mV) = 1.73\ e^-/s$
  - $Well = 81ke^-, 382\ mV$

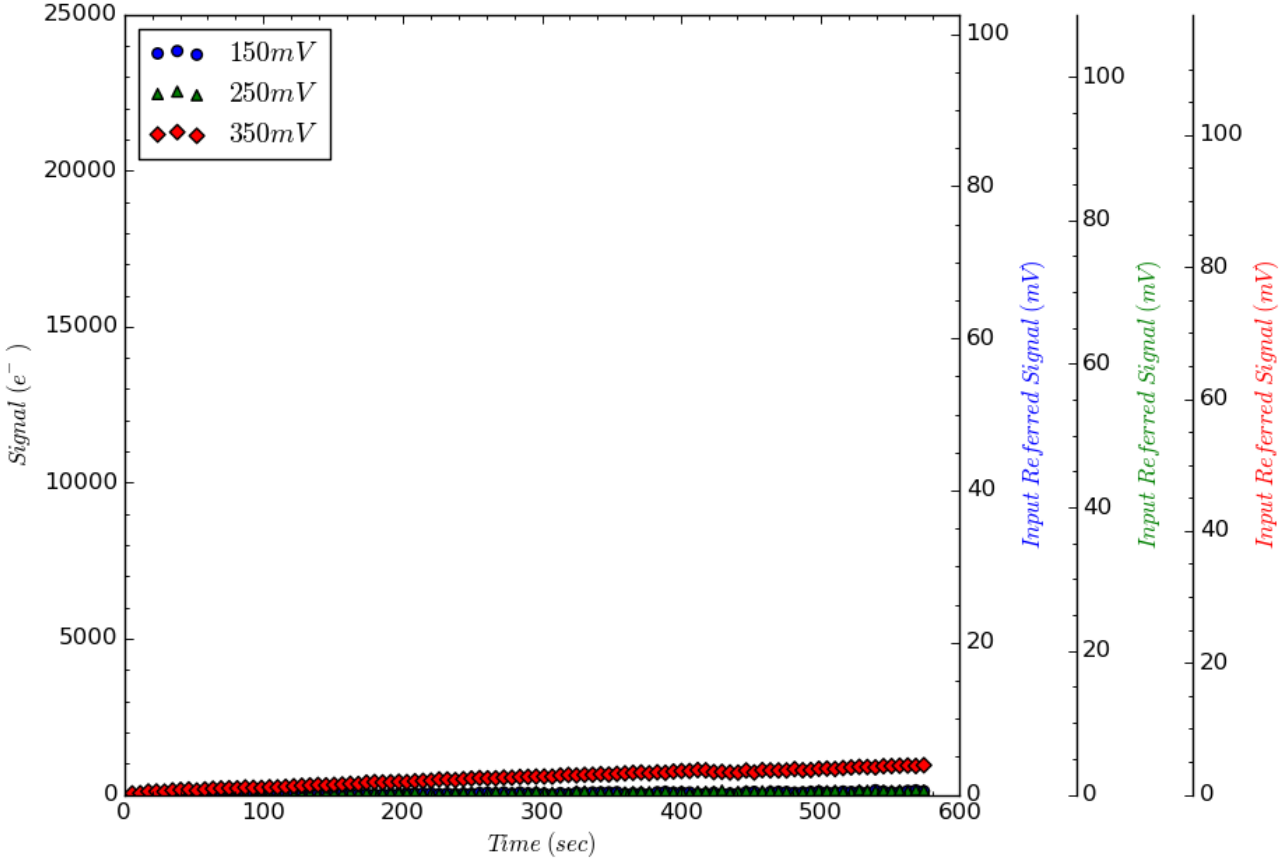

I-T with 250 mV of applied bias

I-V at a temperature of 28 K

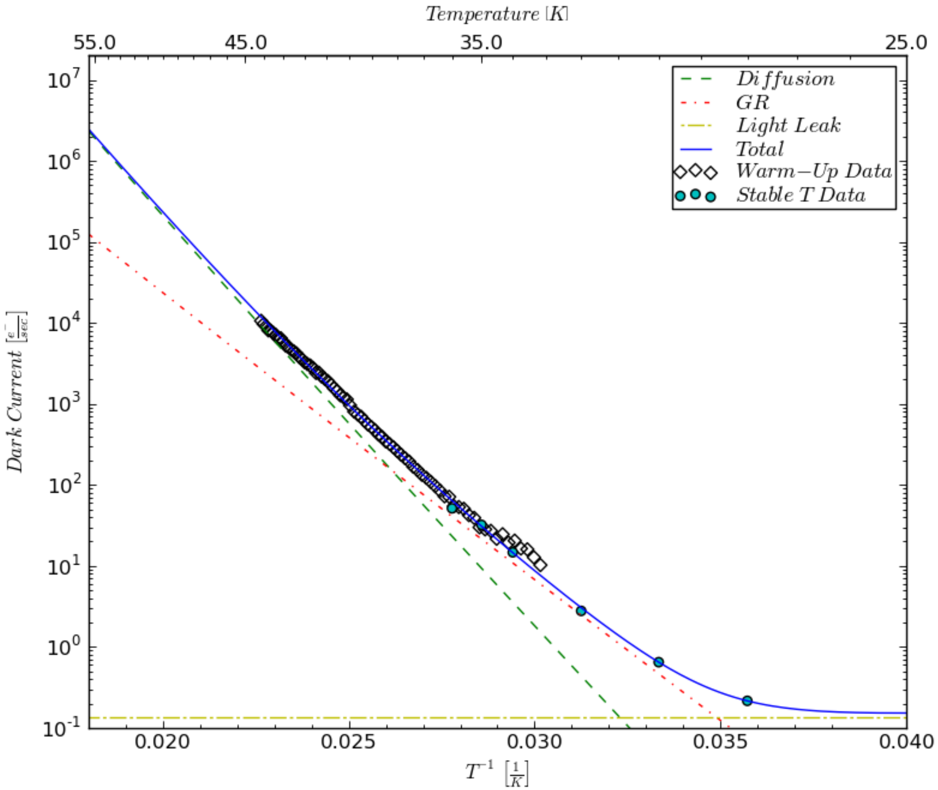

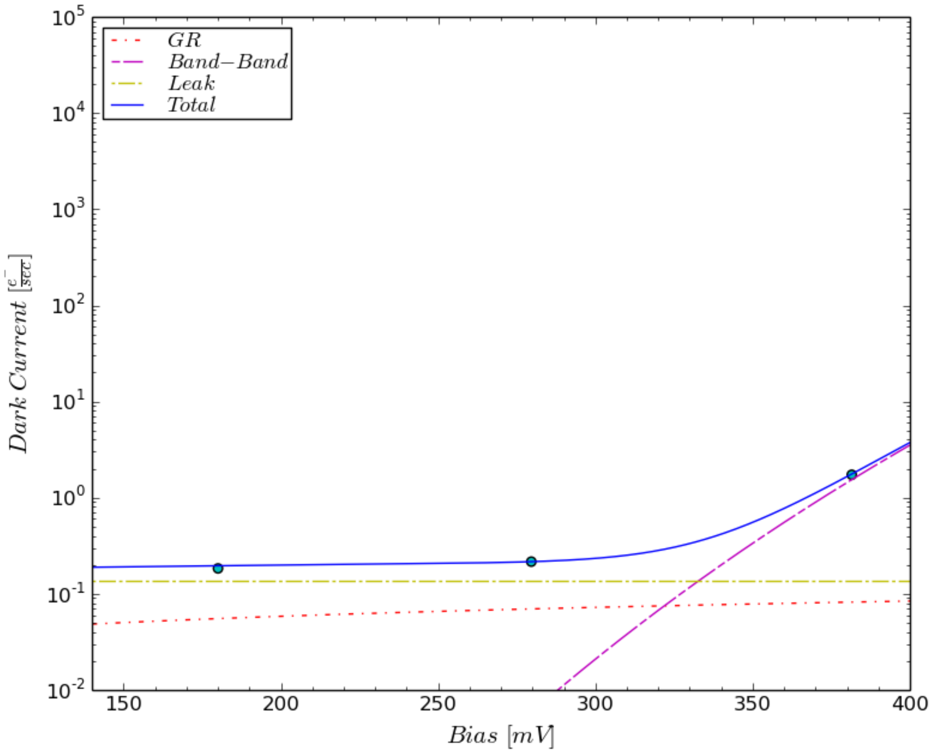

- Dark current model for pixel in previous slide

LW15 RESULTS

- Received three LW15 arrays
  - H1RG-20302 and 20303 were designed to mitigate quantum tunneling dark currents
  - H1RG-20304 was grown and processed in the same manner as the 10 μm arrays for NEOCam
- Tested H1RG-20303
  - Cutoff wavelength of 15.5 μm
  - QE of 83% between 6-12 μm

Dark Current vs. Well Depth

- Lowest dark currents at a temperature of 23K and 50 mV of applied bias
- Median dark current and well depth of $6.22 e^{-}/s$ and $\sim 18 ke^{-}$
- 87.6% of pixels have dark currents < 200 e^{-}/s and well depth greater than $\sim 12 ke^{-}$

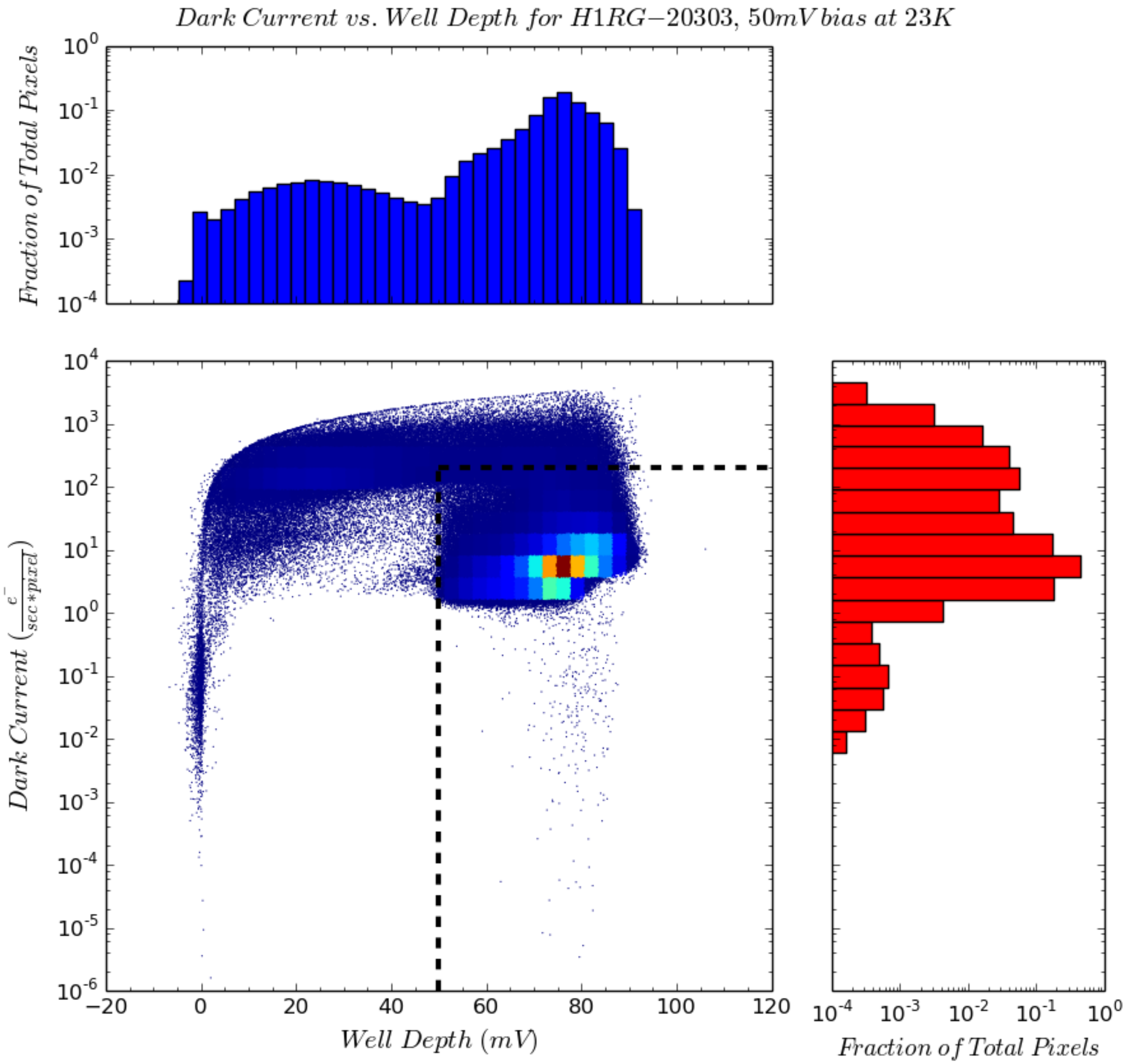

Operability Map

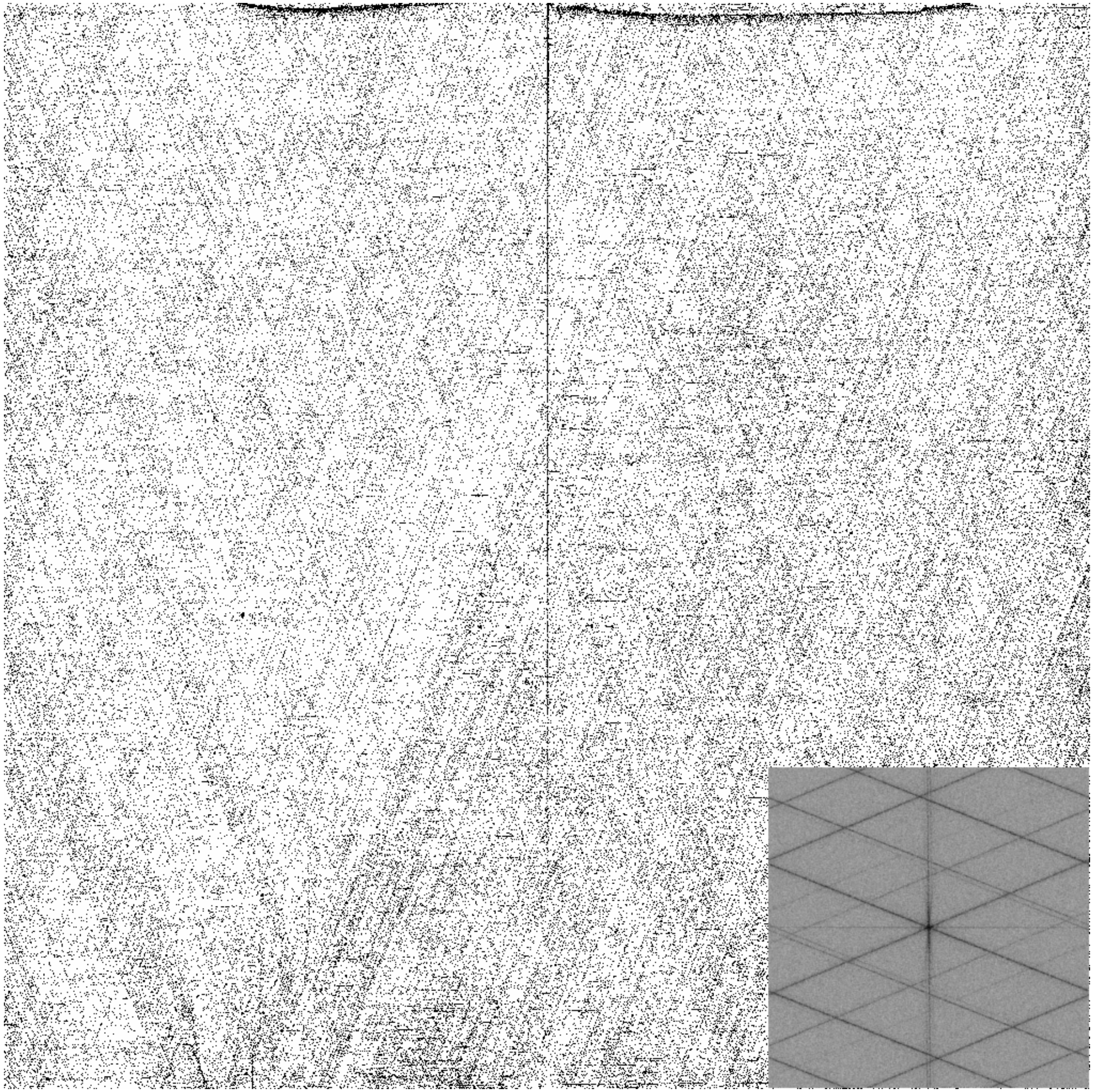

SUTR Curvature

- Increasing bias also increases dark current

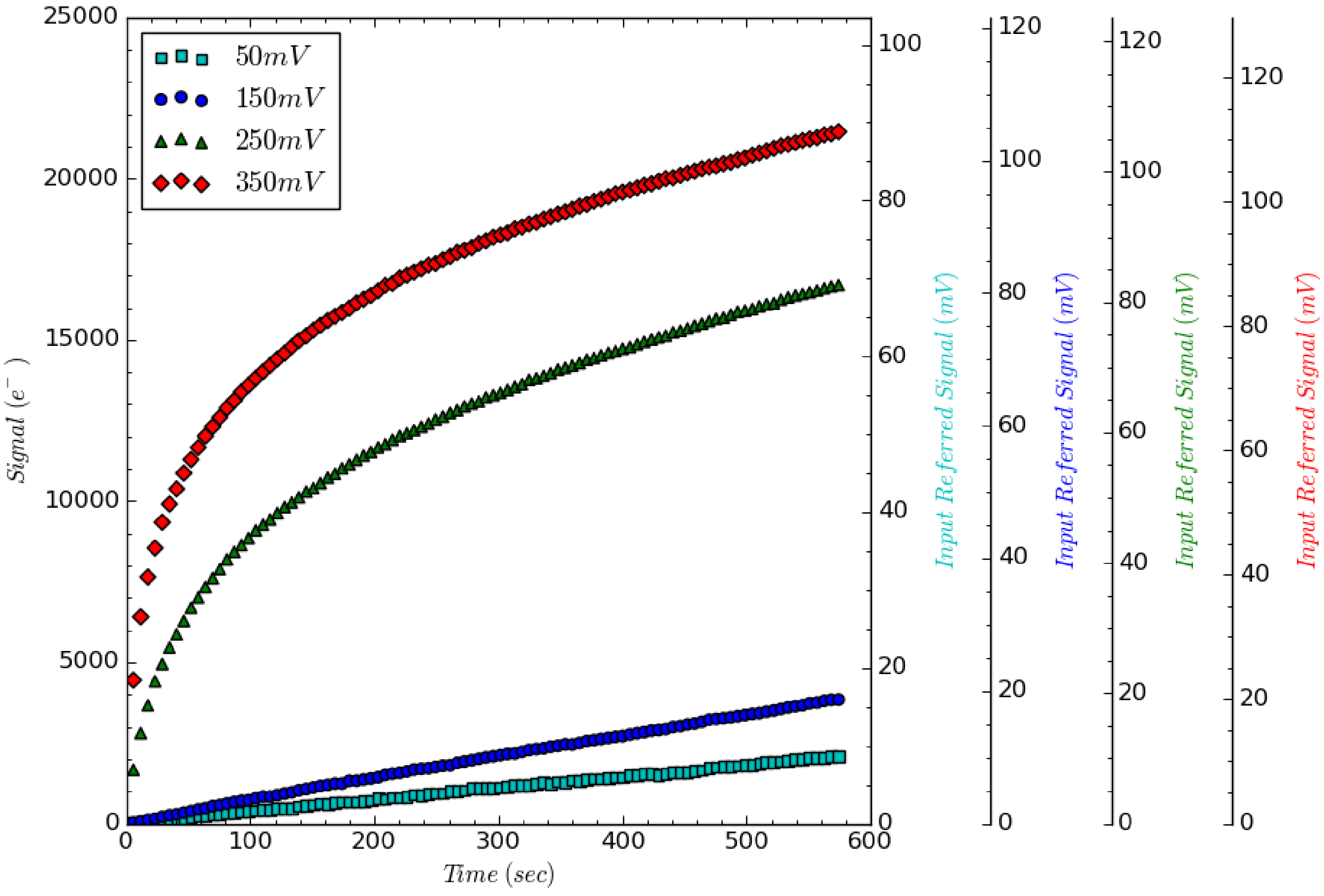

I-T with 150 mV of applied bias

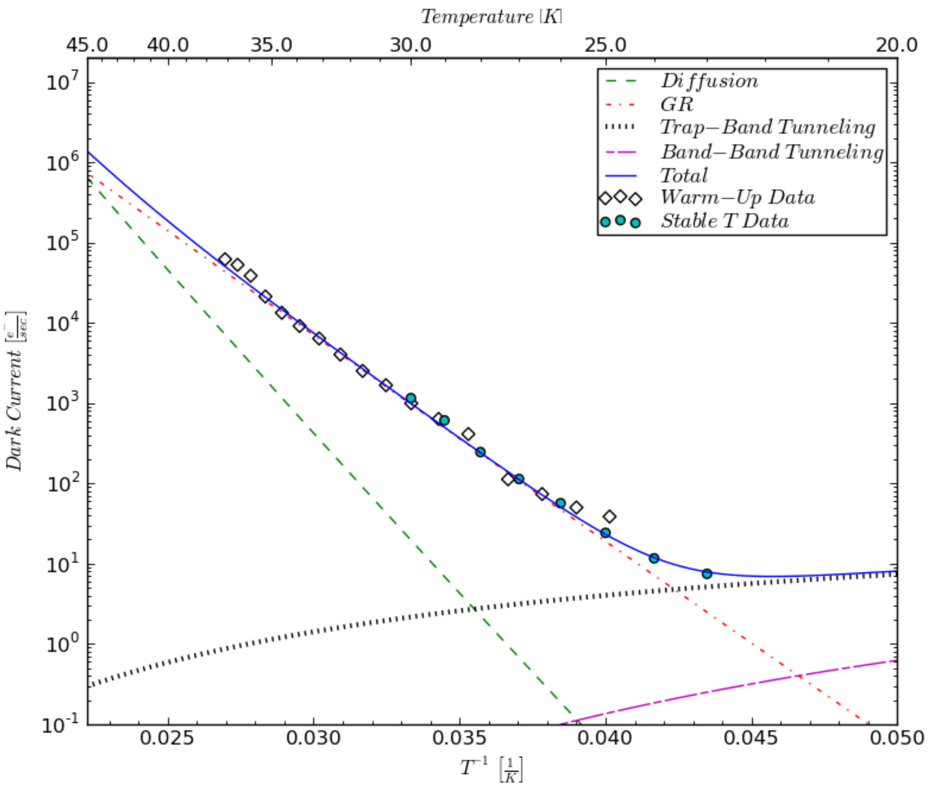

I-V at a temperature of 23 K

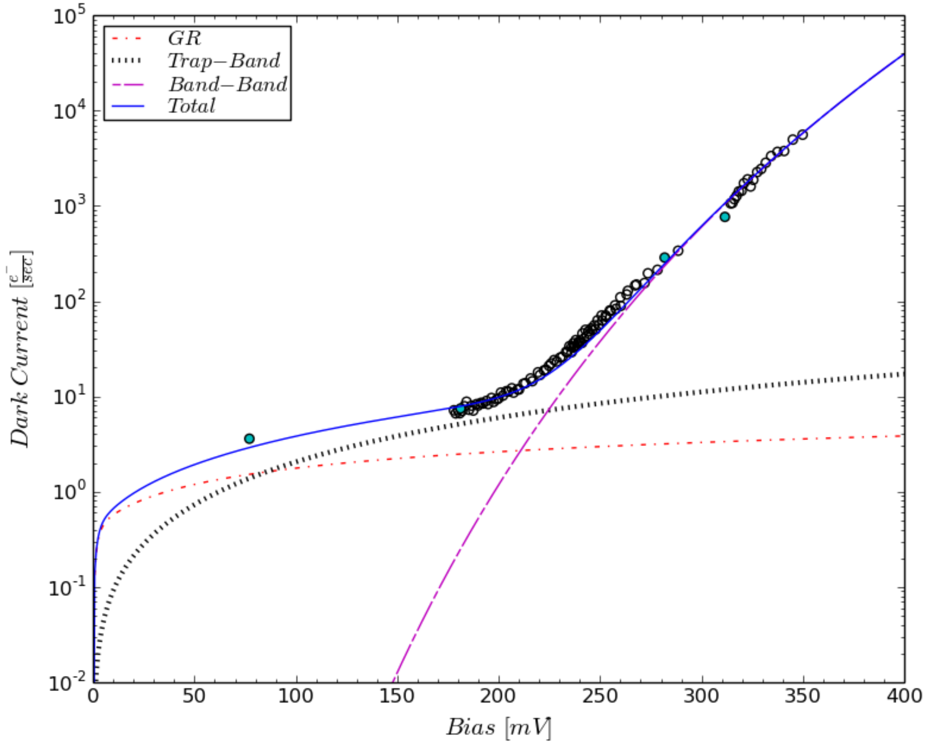

- Dark current model for pixel in previous slide

LW15 Array Summary

- From our fits, we have shown that at 250 and 350 mV of applied bias at a temperature of 23 K, band-to-band tunneling current is the dominating dark current component
- At low temperatures and bias, G-R and trap-to-band appear to dominate dark current
- TIS improved diode structure to reduce band-to-band tunneling

Future Work

- More detailed dark current vs. temperature and bias characterization to determine if the majority of pixels behave similarly as the one presented here
- Characterize two other arrays

Thank you!

QUESTIONS?

References

1. L. Kaltenegger, "How to characterize habitable worlds and signs of life," Annual Review of Astronomy and Astrophysics 55 (1), 433–485 (2017).
2. G. L. Hansen and J. L. Schmit, "Calculation of Intrinsic Carrier Concentration in Hg1−xCdxTe," Journal of Applied Physics 54 (3), 1639–1640 (1983).
3. A. Mainzer, T. Grav, J. Bauer, et al., "Survey simulations of a new near-earth asteroid detec-tion system," The Astronomical Journal 149 (5), 172 (2015).
4. M. Dorn, C. McMurtry, J. Pipher, et al., "A Monolithic 2k x 2k LWIR HgCdTe Detector Array for Passively Cooled Space Missions," Proc. SPIE 10709, 10709 – 10709 – 9 (2018).
5. M. Cabrera, C. McMurtry, M. Dorn, et al., "Development of 13 μm Cutoff Wavelength HgCdTe Detector Arrays for Astronomy," Submitted to the Journal of Astronomical Telescopes, Instruments, and Systems.
6. M. Reine, A. Sood, and T. Tredwell, "Chapter 6 Photovoltaic Infrared Detectors," in Mercury Cadmium Telluride, R. Willardson and A. C. Beer, Eds., Semiconductors and Semimetals 18, 201 – 311, Elsevier (1981).
7. C. T. Sah, R. N. Noyce, and W. Shockley, "Carrier Generation and Recombination in P-N Junctions and P-N Junction Characteristics," Proceedings of the IRE 45 (9), 1228–1243 (1957).
8. S. M. Sze, Physics of Semiconductor Devices, John Wiley & Sons (1981).
9. M. Kinch, "Chapter 7 Metal-Insulator-Semiconductor Infrared Detectors," in Mercury Cadmium Telluride, R. Willardson and A. C. Beer, Eds., Semiconductors and Semimetals 18, 313– 378, Elsevier (1981).
10. M. A. Kinch, State-of-the-Art Infrared Detector Technology, SPIE press Bellingham (2014).